Binding Modes and Pharmacophore Modelling of Thermolysin Inhibitors

M.T.H. Khan*,§, Y. Wuxiuer and I. Sylte

Medical Pharmacology and Toxicology, Department of Medical Biology, Faculty of Health Sciences, University of Tromsø, N-9037, Tromsø, Norway

Abstract: In the present paper 25 known thermolysin inhibitors were docked into thermolysin using the Internal Coordinate Mechanics (ICM™) software. Pharmacophore models based on thermolysin binding modes and activity profiles were generated using the LigandScout™ program. The docking studies indicated that all 25 inhibitors coordinated the catalytic zinc in bidentate or monodentate geometry. A 'three-point' pharmacophore model was proposed which consisted of a hydrophobic group, a negative ionizable group and a hydrogen bond acceptor group. Finally the pharmacophore model has been tested against a small compound library containing 18 highly, moderately, less active as well as inactive compounds. The screening indicated that the pharmacophore model could, identify highly active compounds in front of inactive or less active ones.

Keywords: Thermolysin inhibitors, molecular docking, pharmacophore models, antibacterial drugs, antihypertensive drugs.

INTRODUCTION

Enzymes of the thermolysin (EC 3.4.24.27) family (M4 family of proteinases) are secreted eubacterial endoproteinases from Gram-positive or Gram-negative sources that degrade extracellular proteins and peptides for bacterial nutrition prior to sporulation. The M4 family includes enzymes from pathogens such as *Legionella*, *Listeeria*, *Clostridium*, *Staphyloccus*, *Pseudomonas* and *Vibrio*, and are key factors in the pathogenesis of various diseases, including several types of bacterial infections [1-3], cholera [4], gastritis and peptic ulcer [5, 6] and gastric carcinoma [7].

The protoptype enzyme of the M4 family is thermolysin, which is a 34.6 KDa bacterial Zn-metalloprotease that specifically catalyzes hydrolysis of peptide bonds containing hydrophobic amino acids [8, 9]. Thermolysin is widely used for peptide bond formation through reverse reaction of hydrolysis, and is applied in synthesis of the artificial sweetener aspartame [10, 11]. Thermolysin is also essential for the cellular entry *via* the cell surface of the corona virus (SARS-CoV) which is causing severe acute respiratory syndrome (SARS) [12].

TH structure of thermolysin contains the consensus sequence HExxH that forms the zinc-containing catalytic domain [13, 14]. Zn-metalloproteinases containing the HExxH motif have structural and functional similarities with thermolysin and are often named thermolysin-like proteinases (TLPs). M4 family members are all TLPs. X-ray crystallographic structures of thermolysin [15] and various thermolysin–inhibitor complexes have been used to model the active site of neprilysin (NEP) and angiotensin-converting enzyme (ACE) [16-18]. NEP and ACE are TLPs involved in the control of hypertension [19, 20], and both have large structural and functional similarities with thermolysin.

Enzymes of the M4 family and other TLPs are potential targets for therapeutic intervention. Adequate inhibition of different TLPs is important, especially with the emergent resistance to antibiotics and the fight against multi drug resistance (MDR), and is believed to be a novel strategy in development of second generation antibiotics [21, 22]. Thermolysin may also serve as a model system to identify putative ACE and NEP inhibitors [13, 17]. Structural insight into thermolysin inhibition is therefore important both for the design of putative antibacterial and antihypertensive drugs.

In the present work we report molecular docking and pharmacophore modelling studies of 25 thermolysin inhibitors from the literature. The present results are helpful for designing new thermolysin inhibitors with putative antibacterial or antihypertensive properties.

METHODS

Data Sets and Molecular Structures

In the present study 25 chemically diverse compounds known as thermolysin inhibitors were retrieved from the literature [1, 23]. Biological data (experimental K_i and pK_i values) for the inhibitors is given in Table **1**, and 2D chemical structures in Fig. (**1**). Although the biological data are from different laboratories, the thermolysin inhibition data were considered to be comparable since similar conditions were used during the biochemical experimental studies.

*Address correspondence to this author at the Center for Pharmaceutical Biotechnology (MC 870), College of Pharmacy, University of Illinois at Chicago, Molecular Biology Research Building, 900 South Ashland Avenue, Room 3100, Chicago, IL 60607-7173, USA; Tel: +1-(630)-290-6795; Fax: +1-(312)-413-9303; E-mails: mthkhan2002@yahoo.com, mthkhan2002@gmail.com

§MTHK was a fellow of the "PhD-school in Molecular and Structural Biology" at the University of Tromsø, Norway.

1875-5607/12 $58.00+.00

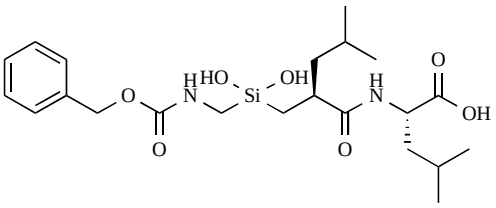

1

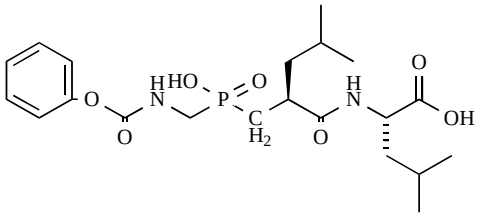

2

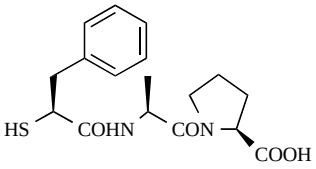

3

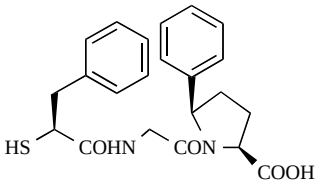

4 (1QF2)

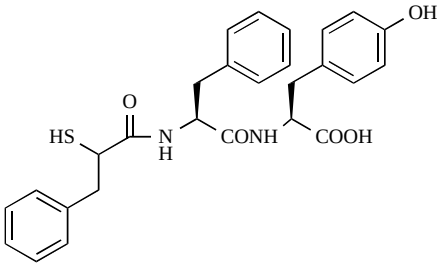

5 (1QF0)

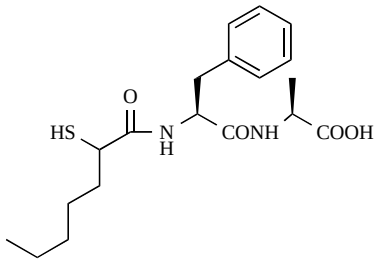

6 (1QF1)

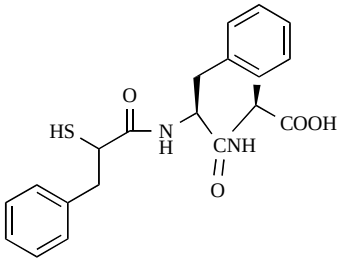

7

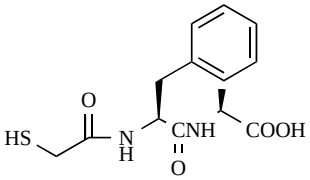

8

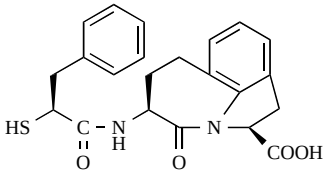

9

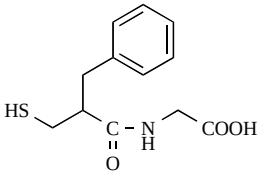

10

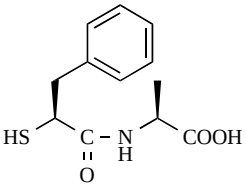

11

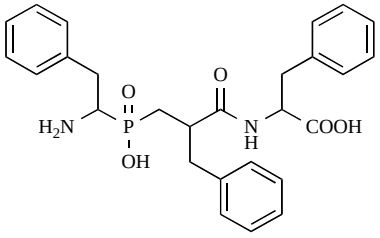

12 (1OS0)

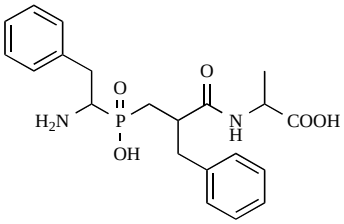

13

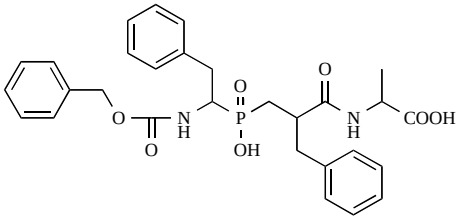

14

(Fig. 2). Contd…..

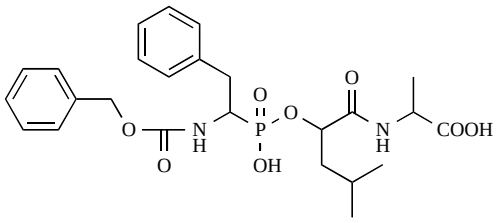

15

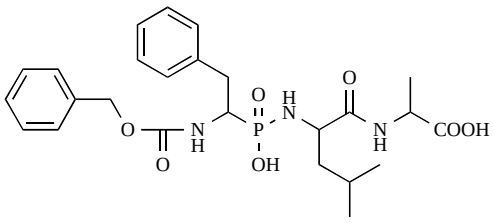

16

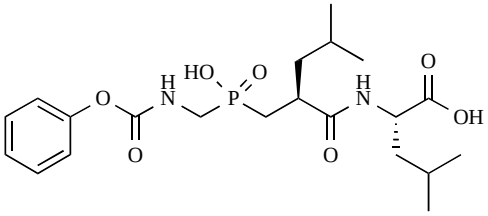

17

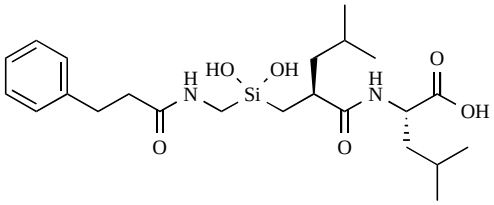

18 (1Y3G)

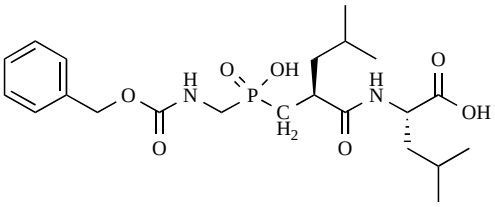

19

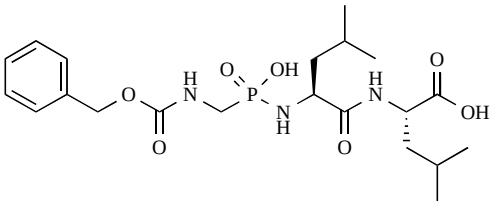

20 (5TMN)

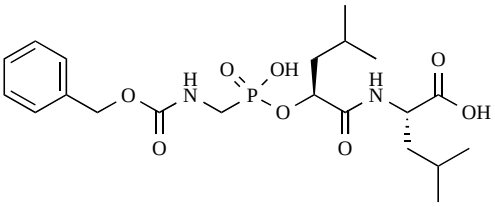

21 (6TMN)

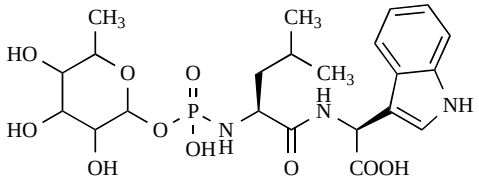

22

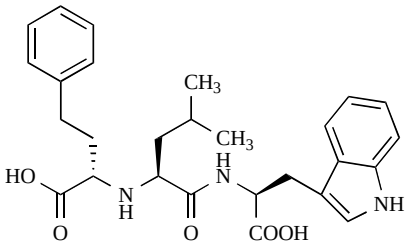

23

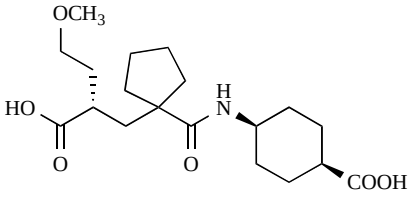

24

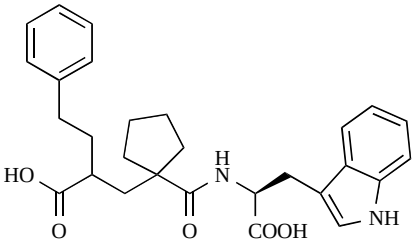

25

Fig. (1). The 2D molecular structures of the thermolysin inhibitors used in this study. The PDB id is given in brackets for compounds that have been co-crystallized with thermolysin.

Table 1. The Experimental *Ki* and p*Ki* Values (Exp. p*Ki*) of the Thermolysin Inhibitors

Comp.	K_i (in M)	Exp. pK_i	Ref.
1	4.1×10^{-8}	7.38722	[1, 23]
2	1.0×10^{-8}	8.0000	[23]
3	2.0×10^{-4}	6.69897	[24]
4	1.2×10^{-3}	5.92082	[24]
5	4.2×10^{-5}	7.37675	[24]
6	4.8×10^{-5}	7.31876	[24]
7	1.9×10^{-5}	7.72125	[24]
8	1.0×10^{-3}	3.00000	[24]
9	1.6×10^{-3}	5.79588	[24]
10	1.6×10^{-3}	5.79588	[24]
11	3.5×10^{-4}	6.45593	[24]
12	9.3×10^{-7}	6.03152	[24]
13	7.8×10^{-7}	6.10791	[24, 25]
14	2.6×10^{-8}	7.58503	[24, 25]
15	4.5×10^{-8}	7.34679	[24, 25]
16	6.8×10^{-11}	10.16749	[24, 25]
17	1.1×10^{-8}	7.95861	[26]
18	4.0×10^{-8}	7.39794	[27]
19	1.0×10^{-8}	8.00000	[27]
20	0.9×10^{-8}	8.04096	[27]
21	9×10^{-3}	2.04576	[27]
22	8.0×10^{-8}	7.09691	[28]
23	5.6×10^{-7}	6.25181	[28]
24	2.2×10^{-6}	5.65561	[28]
25	3.8×10^{-7}	6.42022	[28]

Docking of Thermolysin Inhibitors

Ligand Preparation

Docking of thermolysin inhibitors were performed with the Internal Coordinate Mechanism (ICM™) [29] docking module with default setup. Two-dimensional structures of the 25 inhibitors were drawn using the CS ChemOffice (www.chembridgesoft.com), converted into 3D, energy minimized and saved in PDB format using Discovery Studio (www.accelrys.com). The energy minimized inhibitors were then reposed into ICM environment and converted into ICM objects. MMFF charges [30] were assigned to the inhibitors.

Target Preparation

The X-ray crystal structure of thermolysin (PDB id: 1GXW) was retrieved from Brookhaven Protein databank (PDB, www.rcsb.org/pdb) and converted to ICM-object. The default macro of ICM was used for adding missing hydrogen atoms and for optimizing the thermolysin structure in order to relieve bad van der Waals contacts by a process of short energy minimizations and Monte Carlo simulation. A grid map (5 Å) that included the active site amino acids and zinc was generated. The grid map was manually adjusted.

Docking Process

The previously prepared 25 compounds were docked into the active site of thermolysin (PDB id: 1GXW) using the 'interactive docking' module of ICM. Several docking approaches were tested.

In the first approach Glu143 at the active site was negatively charged while the functionally important histidines at the active site (His142, His146, and His231)

were protonated at the δ-N position. All compounds had a total charge of zero during this docking approach. A stack of complexes (poses) with different orientation and conformation of each compound was sampled. The docking poses were validated based on similarities (RMSD) with known X-ray crystal structures complexes of thermolysin inhibitors in the PDB database (PDB codes: 1QF0, 1QF1, 1QF2, 1THL, 1OS0, 5TMN, 6TMN, 1Y3G) and docking energy. The best ranked docking pose of each compound was refined by a combination of energy minimizations and Monte Carlo simulations of side chains, and the docking energy was again calculated.

It was suggested that the glutamic acid in TLPs corresponding to Glu143 in thermolysin is protonated and interacts with acceptor oxygen of bound ligand [31]. The compounds in Fig. (**1**) that have been co-crystallized with thermolysin (PDB codes: 1QF0, 1QF1, 1QF2, 1THL, 1OS0, 5TMN, 6TMN, 1Y3G) were therefore re-docked in 5 docking runs into two different active site scenarios:

- Scenario 1. Glu143 was negatively charged (as in the first approach).
- Scenario 2. Glu143 was protonated.

The functionally important histidines were still protonated at the δ -N position in both scenarios. The phosphorus based protease inhibitors (Fig. **1**) are acidic, with pKa values in the range of 1.4 - 3.1, and should therefore be charged at physiological pH [1]. All phosphorus based inhibitors from X-ray crystal structure complexes (Fig. **1**) were therefore re-docked both being charged and neutral. All poses from the 5 docking runs of each compound in both scenarios (both charged and neutral for some of the compounds) were analyzed for their similarities with the X-ray structure complexes and docking energy. The analyses indicated that the scenario with neutral Glu143 resulted in docking poses most similar to the X-ray complexes. Further, for the phosphorus based inhibitors, the docking runs with charged compound were most similar to X-ray crystal complexes.

The 17 compounds in Fig. (**1**) that not have been co-crystallized with thermolysin were therefore re-docked with a neutral Glu143 and charged phosphorus groups. Five docking runs were performed for all compounds.

LigPlot [32] was used to construct schematic 2D plots of thermolysin-ligand interactions. Regression analysis between experimental data from the literature and docking calculations were performed by MS Excel™.

Pharmacophore Modeling

Based on an X-ray crystal structure complexes with thermolysin, the highest ranked docking modes of the 25 compounds, and their activity profiles, pharmacophore models were constructed using the program LigandScout™ (www.inteligand.com) version 2.01 [33-38]. The X-ray structure of compound **20** (Fig. **1**) with thermolysin is known (PDB code 5TMN) and the compound is a strong thermolysin binder (K_i value 9.1×10^{-9} M). Compound **20** was therefore used as reference compound for generating pharmacophoric features. The 25 docked complexes were used to generate preliminarily pharmacophore models of each of the molecules. These models were superimposed and merged to produce the most common features. The model common for all 25 complexes were superimposed with the X-ray complex of compound 25, and from that, the final model was proposed. The 3D co-ordinates for the proposed pharmacophoric features were also calculated. The complete approach is schematically indicated in Fig. (**2**).

This proposed model has been further tested using a small library constructed based on from a previous experimental study [39]. In that study we used structure based virtual screening and experimental binding assays to identify 12 thermolysin inhibitors. The library contained 18 compounds of highly active, moderately active, less active and inactive compounds against thermolysin. The pharmacophore model was then used to searching this library in order to see if the model could score strong binders in front weak binders and not binders. The LigandScout™ platform was used for this screening.

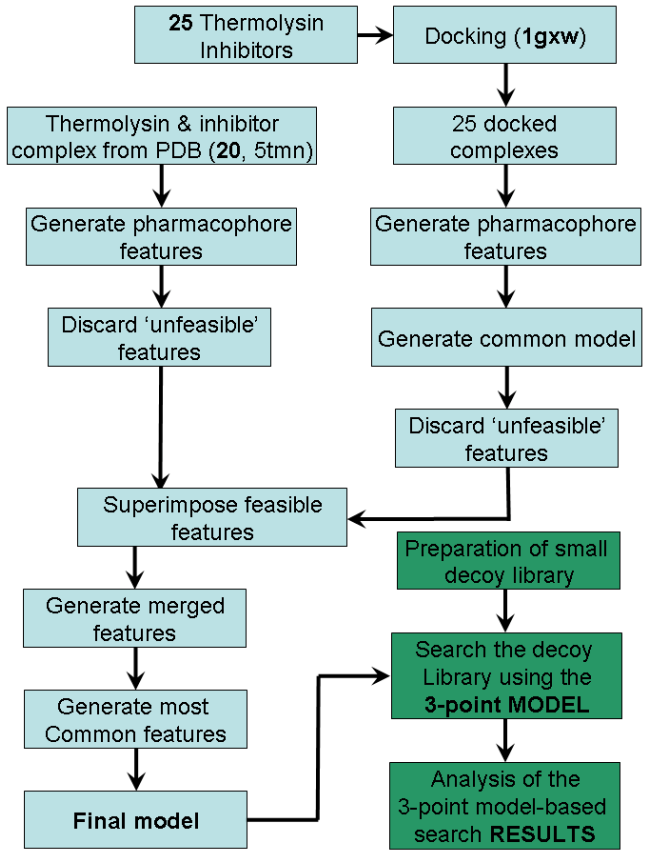

Fig. (2). Schematic representation of the pharmacophore model generation. The model was based on the X-ray structure complex 5tmn and docked complexes of 25 inhibitors. The final model was used to search on a small library (containing 18 compounds).

RESULTS AND DISCUSSION

Therapeutic intervention of TLPs is believed to be a novel strategy in the development of second generation antibiotics and new antihypertensive drugs. Structural insight into binding modes of known thermolysin binders is

therefore important for the design of new thermolysin inhibitors. Computational approaches including docking and scoring and pharmacophore modeling complement experimental studies and may shorten the drug discovery timeline. In the present study computational approaches were used for docking and scoring, and pharmacophore modelling of 25 known thermolysin inhibitors.

Thermolysin – Inhibitor Interactions

Different features including resolution of target X-ray crystallographic structure, ligand conformation, number of rotatable bonds in the ligand, topology and water accessibility of active site, placement of polar hydrogen atoms and correct forms (e.g. charged or uncharged) of ligand(s) and amino acid within the active site have been comprehensively discussed as factors influencing docking accuracy. Several docking programs are available, extensive studies of docking accuracy of different programs during flexible ligand docking have been reported [31, 40-44].

Zinc is essential for biological function and inhibitor binding of thermolysin. Theoretical simulations and ligand affinity predictions of zinc containing proteins are challenging. Zinc can obtain multiple coordination geometries, indicating that the molecular mechanical force field parameters for one molecular system are not directly transferable to other molecular systems, and there it is a lack of force fields capable of reproducing zinc properties. Most docking studies have used a formal charge of +2 for zinc giving relatively low correlation with experimentally obtained affinities, and overestimation of the electrostatic interactions [31]. Table **3** compare docking studies from the literature where different programs have been used to dock compounds with known target-compound X-ray structures. Table **2** indicates that docking into metal containing targets often gives less accurate docking modes compared to targets not containing metal ions.

Bursulaya *et al.* [40] and Hu *et al.* [31] performed docking into 9 and 40 zinc containing targets, receptively. The study by Bursulaya *et al.* [40] indicated that for zinc containing targets, the different programs showed between 1 (Autodock) to 5 (ICM) out of 9 compounds within RMSD of 2 Å from corresponding X-ray complex (Table **3**), while the study by Hu *et al.* [31] had 8 (Dock) to 21 (GOLD) out of 40 zinc containing targets within RMSD of 2 Å. ICM was not used by Hu *et al.* [31] The study by Chen *et al.* did not specifically indicate the accuracy obtained for the zinc containing targets. However, the overall docking accuracy by Chen *et al.* was quite high, especially for the ICM program (91 % within RMSD of 2 Å) and Glide (63 % within RMSD of 2 Å). However, a similar study by Perola *et al.* [43] indicated that ICM reproduced 45 % within RMSD of 2 Å of the X-ray complexes while Glide reproduced 61 %.

An important contribution to the high docking accuracy by Bursulaya *et al.* [40] and Chen *et al.* [41] may be that more than 70 % of the targets did not contain metal ions. However, the results in Table **3** indicate that ICM is a valuable approach for flexible ligand docking, also for zinc containing targets. The docking results of the present study are shown in Table **4** and **5**. Table **5** indicates that the

Table 2. Docking Successfulness Measured by RMSD of Ligand Structure from Corresponding X-Ray Crystal Structure Complex

Ref.	Program	No. of complexes	Percentage[a]		No. of metal containing targets		No. of metal[b]	
			<2.0 Å	<1.0 Å	Total	Zinc	<2.0 Å	<1.0 Å
[40]	Autodock	37	46	24	9	9	1	/
	Dock	37	30	8	9	9	1	/
	FlexX	37	35	11	9	9	2	/
	ICM	37	76	41	9	9	5	2
	GOLD	37	46	22	9	9	3	/
[41]	FlexX	164	43	26	42	34	/	/
	GOLD	164	55	39	42	34	/	/
	GLIDE	164	63	49	42	34	/	/
	ICM	164	91	56	42	34	/	/
[31]	Autodock	40	40	/	40	40	16	/
	Dock	40	20	/	40	40	8	/
	FlexX	40	35	/	40	40	14	/
	DrugScore	40	40	/	40	40	16	/
	GOLD	40	53	/	40	40	21	/

Notes: [a]percentage of compounds within 1 and 2 Å from X-ray complex; [b]No. of metal compounds within 1 and 2 Å from X-ray complex.

docking approach considered as most realistic had 7 out of 8 compounds (87 %) within 2 Å of corresponding X-ray structure complex, while the first approach had 4 out of 8 (50 %).

Several docking approaches were used in the present study. In the first approach all 25 compounds were docked in neutral form with Glu143 of thermolysin negatively charged (Table **3**). Thereafter, the 8 compounds with known X-ray crystal structure complex were re-docked using:

- Protonated (neutral) Glu143, and neutral compounds.
- Protonated Glu143, and with the compounds most probably charged at physiological pH in charged form.

The remaining 17 compounds were then re-docked using protonated Glu143 and compounds most probably charged at physiological pH in charged form. All docking approaches gave rather low correlation between experimental inhibition constants and docking energy for the compounds. The free energy of thermolysin binding was also calculated for the best poses from both docking approaches using the Calc Binding Energy script of ICM [45]. These energies should be more related to the free energy of binding than the docking energy. However, correlation with experimental binding affinities was low.

Low correlation between experimental inhibition constants and docking energy was not unexpected since the compounds have quite diverse chemical structures (Fig. **1**) in the fact that the parameterization of zinc is insufficient. The

Table 3. The Initial Docking of the 25 Compounds (Neutral Compounds). The Energy Values are Given in Kcal/mol

Compound (X-ray complex)	rmsd[a] (Å)	$E_{docking}$[b] (Kcal/mol)	$E_{docking}$[c] (Kcal/mol)	pK_i
1		-131.7	-1095	7.4
2		-82.0	-1068	8.0
3		-79.1	-986.5	3.7
4 (1QF2)	1.93	-91.6	-1042	2.9
5 (1QF0)	1.51	-102.4	-1067	4.4
6 (1QF1)	2.49	-76.7	-1058	4.3
7		-86.1	-1072	4.7
8		-76.1	-1066	3.0
9		-87.0	-1052	2.8
10		-79.6	-1031	2.8
11		-64.2	-1046	3.5
12 (1OS0)	1.31	-112.2	-1118	6.0
13		-105.8	-1116	6.1
14		-136.8	-1106	7.6
15		-122.9	-1073	7.4
16		-127.3	-1015	10.2
17		-106.9	-1069	8.0
18 (1Y3G)	2.49	-118.3	-1082	7.4
19		-109.4	-1029	8.0
20 (5TMN)	1.94	-120.3	-1090	8.0
21 (6TMN)	2.28	-123.9	-1072	2.1
22		-134.8	-1119	7.1
23		-99.7	-976.2	6.3
24		-72.4	-1073	5.7
25 (1THL)	3.75	-112.9	-1069	6.4

Notes: [a]rmsd from corresponding X-ray structure (before refinements) [b]docking energy; [c]energy after refinements.

pose scoring was therefore based on geometrical similarities with known X-ray structures. Table **4** and **5** clearly indicate that using protonated Glu143 and charged compounds resulted in docking poses most similar to the X-ray structures. The remaining 17 compounds were therefore re-docked using this scenario and scored based on the presence of zinc coordination. Docking into metal containing targets is challenging. However, results from the literature (Table **2**) and the present docking (Table **3** and **4**) indicate that using the ICM program is a valuable approach for docking into zinc containing binding sites.

A large number of reported thermolysin inhibitors are dipeptides [24, 28, 46-52], but a number of small organic molecules also inhibit thermolysin. Non-peptide thermolysin inhibitors are most often derivatives of phosphate [24, 25, 53-55], silicon [1], or sulfate [24]. A large number of the thermolysin inhibitors contain common fragments, which bind the catalytic zinc. Nishino and Powers suggested that oxygen atoms present in these fragments may form bidentate interactions with the catalytic zinc ion [56-58] resulting in multiple zinc coordination geometries that play critical roles in the stability of the thermolysin - inhibitor complex [59]. All compounds in the present study contain putative zinc coordinating groups (Fig. **1**). The present docking indicated that all 25 compounds coordinated the catalytic zinc and formed strong interactions. Compounds **22**, **23**, **24** and **25**

Table 4. The Docking Results Using Neutral Glu143 and all Phosphorus Based Inhibitors Charged

Compound (X-ray complex)	NRB	$E_{docking}$[a] (kcal/mol)	Docking pose[b]	
			$E_{docking}$[c] (kcal/mol)	rmsd[d] (Å)
1	16	-124.7	-125.7	
2	15	-107.2	-107.2	
3	9	-70.2	-71.2	
4 (1QF2)	8	-86.4	-81.2	0.37
5 (1QF0)	13	-103.0	-108.5	1.42
6 (1QF1)	13	-88.2	-88.7	0.67
7	11	-88.5	-88.6	
8	9	-70.9	-70.9	
9	6	-82.5	-82.3	
10	7	-66.8	-70.5	
11	6	-65.5	-65.6	
12 (1OS0)	13	-108.8	-111.8	1.55
13	11	-97.4	-97.3	
14	16	-126.7	-125.8	
15	16	-126.6	-124.6	
16	16	-129.9	-130.7	
17	15	-104.6	-104.3	
18 (1Y3G)	16	-111.0	-119.0	2.02
19	16	-118.8	-119.0	
20 (5TM)	16	-108.6	-118.0	1.93
21 (6TM)	16	-106.9	-107.9	2.00
22	11	-128.9	-127.6	
23	14	-104.6	-105.3	
24	10	-84.2	-85.1	
25 (1THL)	12	-99.1	-94.2	1.50

Notes NRB: number of rotatable bonds, [a]Average docking energy for best poses from 5 docking runs; [b]docking energy of the pose closest to the average energy; [c]docking energy of the best pose; [d]rmsd from corresponding X-ray structure.

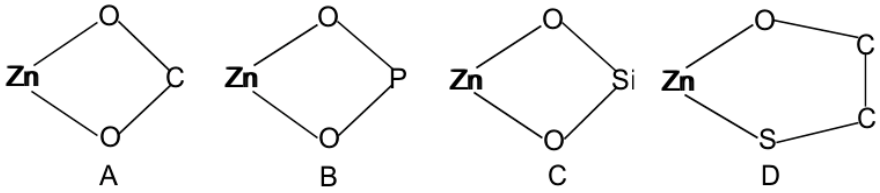

Fig. (3). Geometry of bidentate arrangements of zinc binding groups. **A**: Bidentate arrangements of carboxylate groups give rise to a four membered ring. **B**: Bidentate arrangements of phosphate oxygens groups giving a four membered ring. **C**: Bidentate arrangements of silanediols groups giving a four membered ring. **D**: Bidentate arrangements of OCCS group giving a five membered ring.

coordinated zinc *via* bidentate arrangements of two carboxylate oxygens (OCO) forming a four memberd chelate ring (Fig. **3A**). Compounds **2**, **12**, **13**, **14**, **15, 16**, **17**, **19**, **20** and **21** formed a similar bidentate geometry that included the zinc and phosphate oxygens (OPO) (Fig. **3B**). In addition compound 15 also interacted with zinc *via* amide oxygen (O5). Compound **1** also formed a similar bidentate geometry consisting of oxygens from the O-Si-O group (Fig. **3C**). Compound **18** also formed a similar O-Si-O bidentate, but in addition, the amide oxygen (O1) was also coordinating zinc. Compound **5, 6, 7** and **8** formed a bidentate geometry with zinc *via* oxygen and sulphur of the OCCS group (Fig. **3D**).

All inhibitors interacted with the catalytic zinc of thermolysin (Table **5**). The following section describes additional molecular interactions of the compounds with thermolysin. Atomic numbering is indicated in Fig. (**1**).

Compound 1 (Fig. 4)

Atoms C1, C7 and C9 had hydrophobic interactions with His231, while C4 and C6 interacted with Asn112, Phe130 and Leu202. C10 and C11 interacted with Phe114, C12 with Tyr157 and Trp115, C14 with Asn116, Tyr157 and Trp115. C16 interacted with Asn116, while C17 interacted with Phe114 and Asn116.

Compound 2

Atoms C3, C13, C14, and C15 had hydrophobic interactions with His231, while atoms C5 and C8 interacted with His142. C11 interacted with Phe130, C17 and C18 with Tyr157 and His146, while C19 and C20 interacted with Tyr157.

Compound 3

S1, C4 and C9 interacted with His231. Atom C8 interacted with Asn112, C13 with Leu133 and Phe130, C14 and C15 with Leu133, Phe130, Val139 and Leu202. Atom C16 interacted with Val139 and Leu202, while C17 interacted with Leu202.

Compound 4

The interaction mode of compound 4 was very similar to that of the X-ray crystal structure (PDB id: 1QF2, RMSD: 0.37 Å). S1 had hydrophobic interactions with His231, C4 interacted with Leu133, Phe130 and Val139. Atom C5 interacted with Leu202, C6 and C8 with Phe130, Leu133, Val139 and Leu202. Atom C7 interacted with Leu133, Val139, Leu202 and His231. C9 interacted with His231 and Leu202, C10 with Asn112, C13 and C14 with His231.

Compound 5 (Fig. 4)

S1 showed hydrophobic interactions with Phe114 and His146. Atoms C1, C3, C5, C7, and C8 interacted with Phe114. C4 interacted with Asn112, while C15 with Leu133, Phe130, Leu202 and Ile188. Atoms C16 and C17 interacted with Leu202, Val139, and Ile188. C17 also interacted with Leu133, while C13, C22 and C23 interacted with Phe130, Leu133 and Leu202. Atoms C19 interacted with His231 and Asn112. C27 interacted with His231 and C26 interacted with Phe130. In the x-ray crystal structure (PDB id: 1QF0), C20 interacted with Asn112, C24 and C25 interact with Phe130 and Leu202. Other interaction modes of compound 5 were similar to those in the x-ray crystal structure complex.

Compound 6 (Fig. 4)

The interaction mode of compound 6 was very similar to that of the X-ray crystal structure complex (PDB id: 1QF1). C1, C4 and C5 showed hydrophobic interactions with Phe114. C11 and C13 interacted with Phe130, Leu133, Val139 and Leu202, C14 with Val139, Leu133 and Ile188, C15 with Phe130, Leu133, Val139, Ile188 and Leu202, and C19 with His231.

Compound 7

Atoms S1, C20 and C21 had hydrophobic interactions with Trp115 and Phe114, while S1 and C20 also interacted with Glu166. In addition the following interactions were seen: C3 with His231, C4 with Asn112, C8 with Leu202, C9 and C10 with Leu202, Ile188 and Val139, C10 with His142, C11 and C12 with His142 and Val139, C15, C16, C17 and C18 with Phe114.

Compound 8

S1 showed hydrophobic interactions with Phe114, C3 interacted with His231, C10 and C11 with Phe130, Val139, Leu133 and Leu202, C12 with Phe130, Val139, Leu133, Leu202 and Ile188, and C13 with Val139 and Ile188.

Compound 9

S1, C11 and C14 showed hydrophobic interaction with His231. Atom C16 interacted with His142, C18 and C19 with Val139 and Leu202, C20 with Val139, Leu202 and Phe130, C21 with Phe130, Val139, Leu133 and Leu202.

Compound 10

S1 interacted with His142, His146, His231 and Glu143 (long distant interaction). Atom C3 interacted with His231 and Leu202, C5 with His231, C6 with His142 and His146, C8 with Leu202 and Ile188, C9 with Val139, Leu202, Ile188

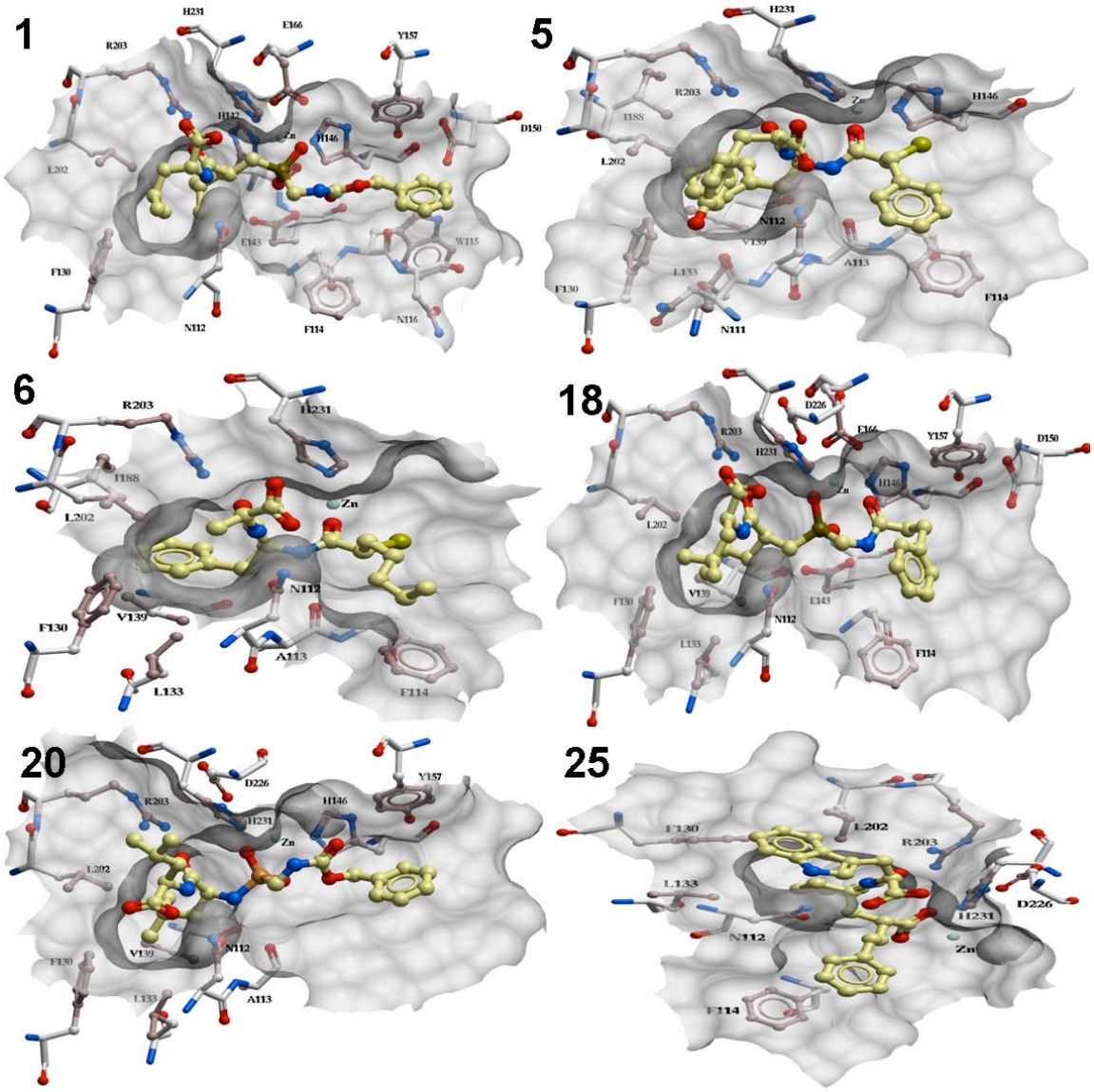

Fig. (4). Three-dimensional view of the molecular interactions of compounds **1, 5, 6, 18, 20** and **25** with active site of thermolysin (PDB code 1gxw). The binding pocket is shown in transparent mode. Interacting amino acids identified by LigPlot [32] analysis are shown. Color coding of atoms: Oxygen: red, nitrogen: blue, sulphur: light green. phosphorous: yellow, zinc: light blue.

and Leu133, C10 with Phe130, Leu202, Val139, Leu133 and Ile188, and C11 with Phe130, Leu133, Val139 and Leu202.

Compound 11

S1 showed hydrophobic interactions with His231 and His142. Atom C3 interacted with Asn112, C6 with His142, C8 and C9 with Ile188, Leu202 and Val139, C10 and C11 with Leu202, Val139, Leu133 and Phe130.

Compound 12

Atoms C1, C3, C4, C5, C6, C7 and C8 all showed hydrophobic interactions with Phe114. Atoms C13, C15 and C17 interacted with Leu133, Leu202, Val139 and Phe130, C16 with Leu133, Leu202 and Val139, C18 with Leu202 and His231, C21 with Asn112, C24 with Leu202, Phe130 and His231. In the x-ray crystal structure complex (PDB id: 1OS0), C14 interacted with His142. Other interactions of compound 12 were similar to those of the x-ray crystal structure complex.

Compound 13

Atoms C1, C2, C3, C4, C6 and C7 showed hydrophobic interactions with Tyr157, Phe114 and His146. Atom C9 showed hydrophobic interactions with His231, while C14 and C15 interacted with Leu202 and Val139. C16 interacted with Leu202, His142, Val139 and Ile188, C17 with Ile188, C18 with Leu202, His142 and Val139 and C21 with Asn112.

Compound 14

C2 and C3 had hydrophobic interactions with Asn112. C4 interacted with Phe114 and Trp115, C13, C14 and C15 with Trp115, Asn116, Gly117 and Tyr157, C16 with Phe114, Trp115 Asn116 and Tyr157, C17 with His142 and His231, C19 with His142 and Leu202, C21 with Leu202,

His142 and Ile188, C22 and C23 with Leu202, His142, Ile188 and Val139.

Compound 15

Atoms C2, C3 and C4 showed hydrophobic interactions with Asn112. Atoms C10, C11, C12, C13, C14, C15 and C16 interacted with Tyr157, C18 and C21 with His142.

Compound 16 (Fig. 5)

Atoms C2 and C3 interacted with Asn112, C4 with Phe114. C10, C12, C14 and C15 with Tyr157, C14 and C15 with Asn116, and C18 and C21 with His142.

Compound 17

Atoms C1, C6, C7 and C8 showed hydrophobic interactions with Leu202. C7 and C8 also interacted with Val139 and Ile188, while C2 interacted with His231. C5 and C8 interacted with His142, while C11, C12 and C13 interacted with Trp115. C12 and C13 also interacted with Tyr157. Finally C17 and C18 interacted with His231.

Compound 18 (Fig. 4)

Atoms C1 and C2 had hydrophobic interactions with His146. C2 and C3 interacted with Tyr157, C8 and C19 with Phe114 and His231, respectively, C15, C16 and C17 with Val139, Leu202, Leu133 and Phe130, C21 with Asn112 and C22 with Leu202 and Phe130. The interaction mode of compound 18 is quite similar to that of the x-ray crystal structure complex (1y3g).

Compound 19

Atom C1 revealed hydrophobic interaction with His231. C7 and C10 interacted with Leu202, C11 and C12 with Leu202, Ile188 and Val139, C11 with Asn112, C12 with His142, C13 with Asn112, C16 with His146 and C18 and C19 with Tyr157.

Compound 20 (Fig. 4)

Atoms C2 and C4 showed hydrophobic interactions with Tyr157 and His146. C13 interacted with Val139, Phe130 and Leu202. C14 and C15 interacted with Val139 and Leu202. C14 also interacted with Leu133 and Phe130, while C18 and C21 interacted with His231. In the x-ray crystal structure (PDB id: 5TMN), C16 and C17 interacted with His231, and not C18 and C21 as indicated by the docked complex. Other interactions were similar to that of the x-ray crystal structure complex.

Compound 21

Atom C1 showed hydrophobic interactions with Tyr157, His146, Phe114 and Asn116. C2 interacted with Tyr157 and His146, C5 and C6 with Phe114 and Asn116, C9 with Phe114 and His146, C13 and C14 with Leu202 and Phe130, C15 and C17 with His231, C17 also with Leu202 and C20 with Asn112, Leu202 and Phe130. In the x-ray crystal structure complex (PDB id: 6TMN), C1 and C2 did not show hydrophobic interactions with His146 as indicated by the docking pose.

Compound 22

Atom C1 interacted with Phe114, C3 with His231, C4 with Tyr157 and His146, C5 with Tyr157 and Phe114, C6 with Phe114 and His146, C9 with Leu202 and Phe130, C10 with Val139, Leu133, Phe130, Leu202 and Asn112, C15 and C16 with Leu202 and Phe130, C17, C18, C19 and C20 with Leu202 and Phe130, while C21 interacted with Asn112.

Compound 23

Atom C1 interacted with His146, His142 and Phe114. C4, C5 and C6 interacted with Phe114 and His146, C8 and C9 with Tyr157 and His146, C16 and C17 with His231, C12 with His142, C24 and C25 with Phe130. C24 also interacted with Asn111, while C26 interacted with Asn112.

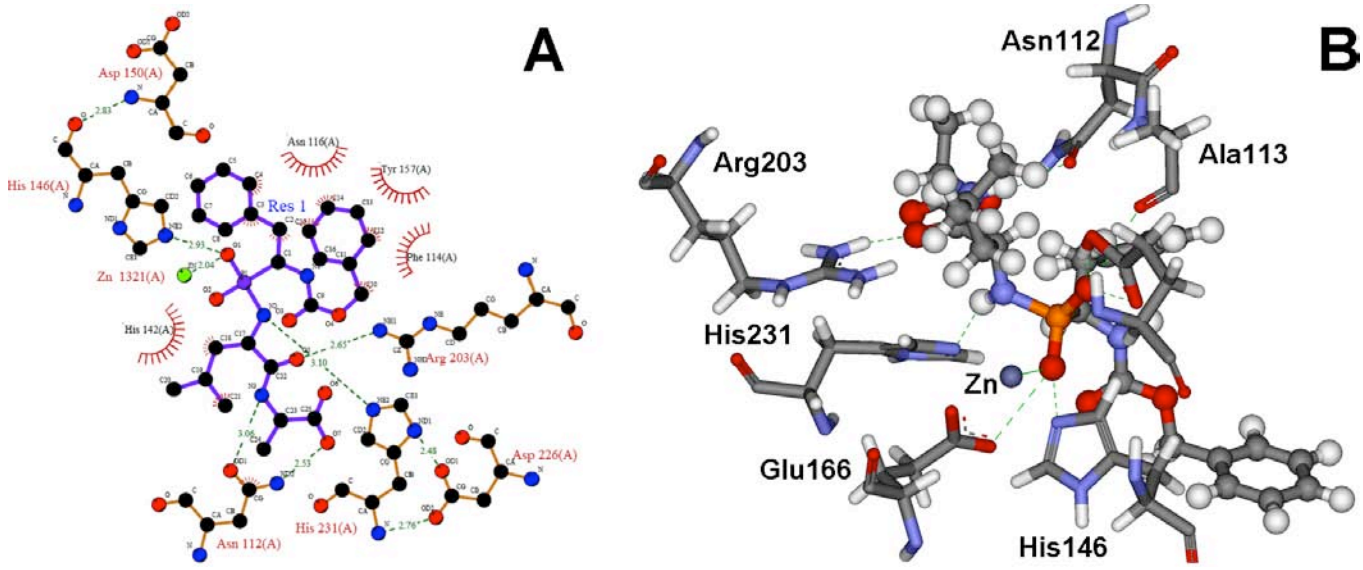

Fig. (5). Molecular interactions of the compound **16**, the most potent inhibitor (Ki = 6.8×10^{-11} M, for detailed see Table **1**) in this work, within the active site of thermolysin (PDB code 1gxw). (**A**) A 2D schematic representation of the interactions (LigPlot), and (**B**) the 3D view of the same interactions, where ball-stick representation is used for compound **16** and purple CPK sphere model representation is used for the Zn ion.

Table 5. Interatomic Distances Between Amino Acids in Thermolysin and Functionally Important Groups of the Compounds

Compound	Atomic dist. to Zn		Hydrogen bonding interactions		
	Comp. atom	Dist. (Å)	Comp. atom	Thermolysin atom	Dist. (Å)
1	O4	2.6	N1	Asn112 (OD1)	3.2
	O5	2.3	O3	Arg203 (NH1)	2.8
			O4	Glu143 (OE1)	2.6
			O5	His146 (NE2)	2.9
			O5	Glu166 (OE2)	2.6
			O6	Trp115 (N)	3.3
2	O2	2.3	O2	His146 (NE2)	3.3
	O3	3.7	O4	Arg203 (NH1)	2.6
			N2	Asn112 (OD1)	3.2
3	S1	2.7	S1	His231 (NE2)	3.2
			O2	Asn112 (ND2)	2.5
			O3	Arg203 (NH1)	2.3
			O3	Arg203 (NH2)	3.2
			N2	Asn112 (OD1)	3.3
4	S1	2.6	O1	Arg203 (NH1)	2.4
			O1	Arg203 (NH2)	3.3
			N1	Asn112 (OD1)	3.1
			O2	Asn112 (ND2)	2.7
5	O1	1.9	N1	Ala113 (O)	3.1
	S1	3.7	O2	Arg203 (NH1)	3.0
			O2	Arg203 (NH2)	3.1
			O3	Asn111 (O)	3.0
			O5	Asn112 (ND2)	2.6
6	O1	2.1	N1	Asn112 (OD1)	3.1
	S1	3.9	N1	Ala113 (O)	3.0
			N2	Asn112 (OD1)	3.0
			O2	Arg203 (NH1)	3.0
			O2	Arg203 (NH2)	3.2
			O4	Asn112 (ND2)	2.7
7	S1	2.3	S1	His146 (NE2)	3.2
	O4	2.4	N2	Asn112 (OD1)	2.9
			O4	His142 (NE2)	3.0
8	O3	2.1	N1	Asn112 (OD1)	3.3
	S1	4.0	N2	Asn112 (OD1)	3.0
			O1	Asn112 (ND2)	2.5
			O2	Arg203 (NH1)	2.7
			O2	Arg203 (NH2)	3.1

(Table 5). Contd…..

Compound	Atomic dist. to Zn		Hydrogen bonding interactions		
	Comp. atom	Dist. (Å)	Comp. atom	Thermolysin atom	Dist. (Å)
9	S1	2.5	S1	His231 (NE2)	3.2
			O2	Asn112 (ND2)	2.4
			O3	Arg203 (NH1)	2.5
			O3	Arg203 (NH2)	2.9
10	S1	2.5	N1	Asn112 (OD1)	3.3
			O1	Asn112 (ND2)	2.5
			O2	Arg203 (NH1)	2.7
			O2	Arg203 (NH2)	3.3
11	S1	2.4	S1	His142 (NE2)	3.3
			N1	Asn112 (OD1)	3.1
			O1	Asn112 (ND2)	2.5
			O2	Arg203 (NH1)	2.7
			O2	Arg203 (NH2)	3.2
12	O1	2.5	N1	Glu143 (OE1)	3.3
	O2	2.2	N2	Asn112 (OD1)	3,1
			O1	His231 (NE2)	3.3
			O2	His146 (NE2)	3.1
			O2	His142 (NE2)	3.2
			O3	Arg203 (NH1)	2.7
			O5	Asn112 (NH1)	2.5
13	O1	2.1	N2	Asn112 (OD1)	3.1
	O2	3.6	O1	His231 (NE2)	3.1
			O3	Arg203 (NH1)	2.6
			O5	Asn112 (ND2)	2.6
14	O1	2.1	O1	His146 (NE2)	3.0
	O2	3.4	N2	Asn112 (OD1)	3.1
			O5	Arg203 (NH1)	2.7
			O7	Asn112 (ND2)	2.6
15	O1	2.1	O1	His146 (NE2)	3.0
	O2	3.7	N2	Asn112 (OD1)	3.1
	O5	3.1	O5	His231 (NE2)	3.2
			O6	Arg203 (NH1)	2.6
			O8	Asn112 (ND2)	2.6
16	O1	2.0	O1	His146 (NE2)	2.9
	O2	3.6	N2	His231 (NE2)	3.1
			N3	Asn112 (OD1)	3.1
			O5	Arg203 (NH1)	2.6
			O7	Asn112 (ND2)	2.5

(Table 5). Contd…..

Compound	Atomic dist. to Zn		Hydrogen bonding interactions		
	Comp. atom	Dist. (Å)	Comp. atom	Thermolysin atom	Dist. (Å)
17	O4	2.5	O2	Arg203 (NH1)	2.7
	O5	2.4	O3	Arg203 (NH1)	2.7
			O3	Arg203 (NH2)	3.0
			O4	His231 (NE2)	2.9
			O5	His142 (NE2)	3.0
			N2	Ala113 (O)	3.2
			N2	Asn112 (OD1)	3.0
18	O1	2.7	O1	His146 (NE2)	2.8
	O2	2.5	O2	Glu143 (OE1)	2.6
	O3	2.6	O3	His231 (NE2)	2.6
			O4	Arg203 (NH1)	2.6
			O4	Arg203 (NH2)	3.1
			O5	Arg203 (NH1)	2.8
19	O4	2.6	O1	Asn112 (ND2)	2.6
	O5	2.8	O3	Arg203 (NH1)	2.6
			O3	Arg203 (NH2)	3.3
			O4	His231 (NE2)	3.0
			N2	His231 (NE2)	3.0
20	O3	2.5	N2	Ala113 (O)	3.3
	O4	2.5	N2	Asn112 (OD1)	3.1
			N3	Asn112 (OD1)	3.3
			O4	His231 (NE2)	2.7
			O5	Arg203 (NH1)	2.6
			O5	Arg203 (NH2)	3.0
			O7	Asn112 (ND2)	2.4
21	O3	2.5	N1	Glu143 (OE1)	3.1
	O4	2.6	O1	Trp115 (N)	3.0
			O4	His231 (NE2)	2.6
			O6	Asn112 (ND2)	2.7
			O8	Arg203 (NH1)	2.5
22	O2	2.5	O1	His142 (NE2)	2.3
	O7	3.0	O1	His146 (NE2)	2.8
			O2	His231 (NE2)	2.8
			N2	Asn112 (OD1)	2.9
			O6	Trp157 (O)	2.7
			O7	Glu143 (OE1)	2.7
			O8	Arg203 (NH1)	3.1
			O10	Asn112 (ND2)	2.7

(Table 5). Contd…..

Compound	Atomic dist. to Zn		Hydrogen bonding interactions		
	Comp. atom	Dist. (Å)	Comp. atom	Thermolysin atom	Dist. (Å)
23	O1	2.3	N1	His231 (NE2)	3.0
	O2	2.3	N3	Asn111 (O)	2.8
			O3	Arg203 (NH1)	2.4
			O3	Arg203 (NH2)	3.2
			O5	Asn112 (ND2)	3.2
24	O1	2.1	O1	Hi231 (NE2)	2.9
	O2	2.3	O2	His146 (NE2)	3.2
			O3	Arg203 (NH1)	2.2
			O4	Arg203 (NH2)	3.1
25	O1	2.4	O1	His231 (NE2)	3.2
	O2	2.2	O3	Arg203 (NH1)	2.7
			O5	Asn112 (ND2)	2.7

Notes: Hydrogen bonding distances ≤ 3.3 Å and zinc binding distances ≤ 4 Å are included in the table.

Compound 24

Atom C5 interacted with Asn112, C19 interacted with Asn112 and His146. C8 interacted with His142, while C9, C10, C11 and C12 interacted with Leu202. C9, C11 and C12 also interacted with His231, and C18 interacted with Phe114.

Compound 25 (Fig. 4)

Atoms C3 and C11 interacted with Asn112. Atoms C4, C5, C6, C7, C8 and C9 interacted with Phe114. C13 and C14 interacted with Leu202, while C14 also interacted with Phe130 and Asn112. C16 showed interaction with Leu133, C18 and C19 with His231, and C27 and C28 with Leu202 and Phe130. The hydrophobic interaction mode of this compound was similar to that of the x-ray crystal structure complex (PDB id: 1thl).

Pharmacophore Modeling

It has been concluded that LigandScout™ is a valuable and effective tool in drug discovery [33-38]. In the present study, the LigandScout™ program was used to perform pharmacophore modelling based on the available X-ray crystal structure complex of compound 20 (PDB id: 5TMN), binding modes obtained by the second docking approach (neutral Glu143 and all phosphorous compounds charged) and the experimental profiles of the inhibitors. Fig. (**6**) shows the close up of the active site interactions of compound **20** (PDB code 5TMN). Compound **20** is a strong thermolysin inhibitor (K_i = 9.1×10^{-9} M), and the X-ray the complex was used as a template for pharmacophore modelling.

The key interactions in this complex were considered as the main pharmacophoric features and have been illustrated in Fig. (**7**), where unfavorable (gray spheres) and favorable (others than gray spheres) features for the complexation are shown. All docked complexes from the second docking approach were analyzed in a similar manner, and thereafter the favorable and unfavorable features were superimposed. The most common and favorable features were then chosen as putative pharmacophoric features (Fig. **8**).

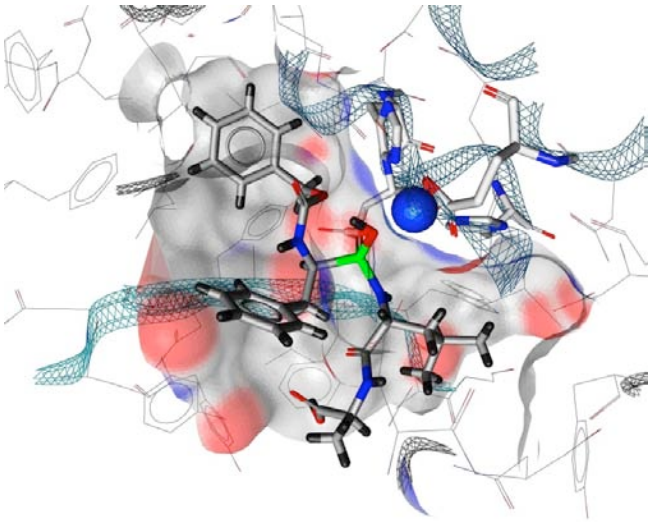

Fig. (6). 3D view of the X-ray structure complex of compound **20** with thermolysin (PDB code: 5TMN) indicating the chemical features that characterizes the specific interaction mode of compound **20** at the active site pocket. The blue CPK sphere represents the catalytic zinc. MMFF94 charges of the atoms are used to represent the surface of the target.

The calculations suggested a three-point pharmacophore model consisting of a hydrophobic, a negative ionizable and a hydrogen bonding accepting group. Their atomic coordinates in 3D space are given in Fig. (**8**). For the strongest binder (compound **16**) these groups correspond to the benzene ring (C11-C16), the phosphate group, and the

oxygen (O3) of an amide group (Fig. **1**), respectively. In the docked complex of compound 16, the atomic distance between P and C11 was 6.7 Å, the atomic distance between P and O3 was 3.7 Å, while the distance between O3 and C11 was 4.2 Å.

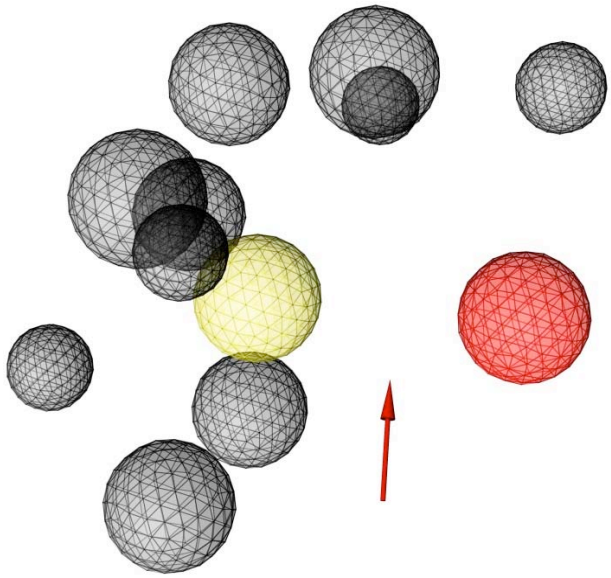

Fig. (7). The best pharmacophore models based on the activity profile, using compound **20** (K_i = 9.1×10^{-9} M) as reference. Grey spheres represent excluded volume, the yellow sphere is hydrophobic, red is negative ionizable, while red arrow represent hydrogen bonding acceptor group.

The final model shown in Fig. (**8**) has then been tested against a small library of 18 compounds containing highly active, moderately active, less active and inactive compounds against thermolysin using the LigandScout™ platform. During the search the model also included the undesirable volumes (shown in Fig. **7**), in addition to the features shown in Fig. (**8**). The results are given in Table **6**, which shows the activity profiles (the IC_{50} values, in mM) from our previous experimental study [39], if the compound matches the model or not, the number of matching features between the model and the compound, and the RMSD values between the model and the compound for the matching featurs.

The screening process identified that 8 of the 12 thermolysin binders contained the pharmacophoric features. The most active compounds were all matching the pharmacophoric features consisting of a hydrophobic, a negative ionizable and a hydrogen bond acceptor group, while some of the least active compounds (IC_{50} values 299.1, 91.6, 29.5 and 14.5 mM) did not. However, the screening process also indicated that 5 out of 6 compounds shown not to bind thermolysin [39] were matching the features of the 3-point pharmacophore model. The screening process showed that the 3-point pharmacophore model was able to identify thermolysin binders, since 8 of 12 compounds known to bind thermolysin matched the pharmacophoric features, indicating that structure-based pharmacophore modelling is a novel approach in search for new thermolysin binders. However, the model failed in identifying compounds not binding thermolysin, since 5 out the 6 compounds known not to bind thermolysin also were in agreement with the pharmacophoric features. A reason for that may be that the 6 compounds were quite similar in structure. Although this model have limitations, it would be interesting to perform a similar search using a larger library.

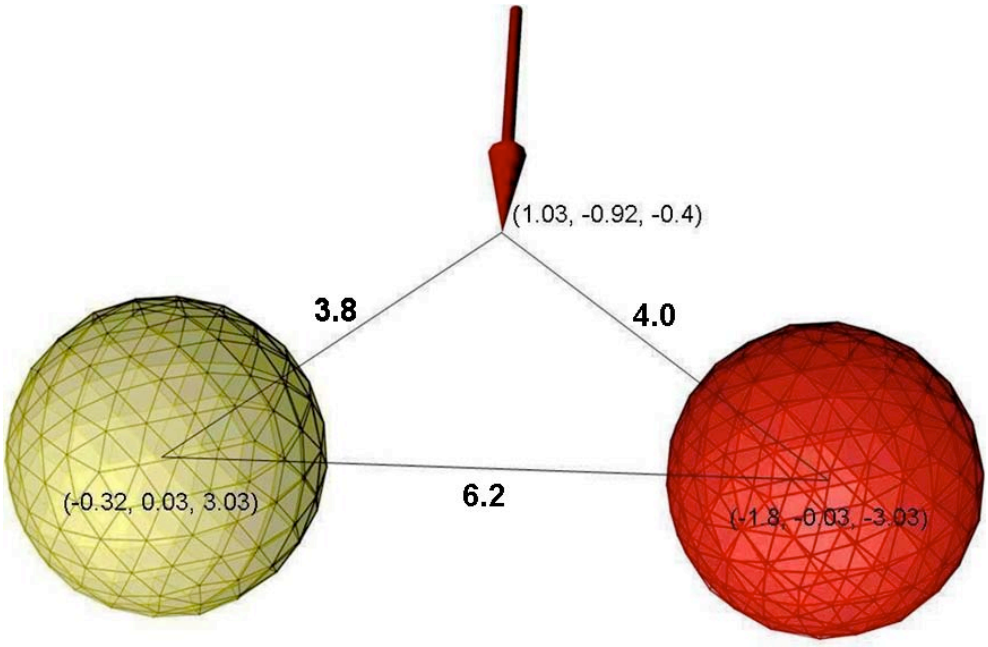

Fig. (8). The proposed three-point pharmacophore model, without excluded volumes. Yellow sphere represents a hydrophobic group, red a negative ionizable group and the red arrow represent hydrogen bond accepting group. Co-ordinates in 3D space are given in parentheses. The distances between the three points are given in Ångstrøm.

Table 6. Pharmacophore Search Results of the 3-Point Model Against Small Decoy Library

Comp.	IC_{50} values (in mM)[39]	Pharmacophore Matching	Matched Features pairs	RMS (Matchedfeatures pairs)
L01	294.06	No	-	-
L02	81.41	Yes	5	0.741
L03	161.14	Yes	4	0.79
L04	IA	Yes	5	0.74
L05	697.48	Yes	4	1.124
L06	48.13	Yes	4	0.556
L07	LA	Yes	4	0.945
L08	6.4×10^{-08}	Yes	5	0.794
L09	IA	Yes	5	0.794
L10	IA	No	-	-
L11	IA	Yes	3	0.883
L12	91.57	No	-	-
L13	IA	Yes	3	0.258
L14	0.35	Yes	4	1.106
L15	14.54	No	-	-
L16	29.5	No	-	-
L17	0.047	Yes	3	0.975
L18	20.58	Yes	5	0.586

Notes: A = active; LA = due to less activity IC_{50} value was not possible to calculate; IA = inactive.

CONCLUSION

Docking programs should be able to identify novel 'binders' as accurate as possible. However, docking into zinc containing binding sites is a challenge due to lack of force fields capable of reproducing zinc properties. The present study indicates that ICM is a valuable tool for docking into zinc containing binding sites, but more precise parameters for reproducing zinc interaction properties should be developed. The docking showed that the compounds coordinated the catalytic zinc in a bidentate or monodentate manner. This study can assists in the design of novel and potent thermolysin inhibitors, which could be used as lead compounds for the advancement of antihypertensives (*e.g.*, ACE and NEP inhibitors) and antibacterials.

CONFLICT OF INTEREST

None declared.

ACKNOWLEDGEMENT

None declared.

REFERENCES

[1] Kim SJ, Kim DH, Park JD, Woo JR, Jin Y, Ryu SE (2003) Origin of the stereospecificity in binding hydroxamates of alpha- and beta-phenylalanine methylamide to thermolysin revealed by the x-ray crystallographic study. Bioorg Med Chem 11(11):2421-2426.

[2] Mariencheck WI, Alcorn JF, Palmer SM, Wright JR (2003) Pseudomonas aeruginosa elastase degrades surfactant proteins a and d. Am J Respir Cell Mol Biol 28(4):528-537.

[3] Hobden JA (2002) Pseudomonas aeruginosa proteases and corneal virulence. DNA Cell Biol 21(5-6):391-396.

[4] Naka A, Yamamoto K, Miwatani T, Honda T (1992) Characterization of two forms of hemagglutinin/protease produced by vibrio cholerae non-o1. FEMS Microbiol Lett 77(1-3):197-200.

[5] Schmidtchen A, Holst E, Tapper H, Bjorck L (2003) Elastase-producing pseudomonas aeruginosa degrade plasma proteins and extracellular products of human skin and fibroblasts, and inhibit fibroblast growth. Microb Pathog 34(1):47-55.

[6] Schmidtchen A, Wolff H, Rydengard V, Hansson C (2003) Detection of serine proteases secreted by lucilia sericata *in vitro* and during treatment of a chronic leg ulcer. Acta Derm Venereol 83(4):310-311.

[7] Veber DF, Johnson SR, Cheng HY, Smith BR, Ward KW, Kopple KD (2002) Molecular properties that influence the oral bioavailability of drug candidates. J Med Chem 45(12):2615-2623.

[8] Morihara K and Tsuzuki H (1970) Thermolysin: Kinetic study with oligopeptides. Eur J Biochem 15(2):374-380.

[9] Inouye K, Lee SB, Tonomura B (1996) Effect of amino acid residues at the cleavable site of substrates on the remarkable activation of thermolysin by salts. Biochem J 315 (Pt 1):133-138.

[10] Oyama K, Kihara K, Nonaka Y (1981) Synthesis of an aspartame precursor by immobilized thermolysin in an organic solvent. J. Chem. Soc., Perkin Trans., II:356–360.

[11] Inouye K (1992) Effects of salts on thermolysin: Activation of hydrolysis and synthesis of n-carbobenzoxy-l-aspartyl-l-

phenylalanine methyl ester, and a unique change in the absorption spectrum of thermolysin. J Biochem 112(3):335-340.

[12] Matsuyama S, Ujike M, Morikawa S, Tashiro M, Taguchi F (2005) Protease-mediated enhancement of severe acute respiratory syndrome coronavirus infection. Proc Natl Acad Sci U S A 102(35):12543-12547.

[13] Roques BP (1993) Zinc metallopeptidases: Active site structure and design of selective and mixed inhibitors: New approaches in the search for analgesics and anti-hypertensives. Biochem Soc Trans 21 (Pt 3)(3):678-685.

[14] Roques BP, Noble F, Dauge V, Fournie-Zaluski MC, Beaumont A (1993) Neutral endopeptidase 24.11: Structure, inhibition, and experimental and clinical pharmacology. Pharmacol Rev 45(1):87-146.

[15] Holmes MA and Matthews BW (1982) Structure of thermolysin refined at 1.6 a resolution. J Mol Biol 160(4):623-639.

[16] Tiraboschi G, Jullian N, Thery V, Antonczak S, Fournie-Zaluski MC, Roques BP (1999) A three-dimensional construction of the active site (region 507-749) of human neutral endopeptidase (ec.3.4.24.11). Protein Eng 12(2):141-149.

[17] Bohacek RS, McMartin C, Guida WC (1996) The art and practice of structure-based drug design: A molecular modeling perspective. Med Res Rev 16(1):3-50.

[18] Turner AJ, Isaac RE, Coates D (2001) The neprilysin (nep) family of zinc metalloendopeptidases: Genomics and function. Bioessays 23(3):261-269.

[19] Wyvratt MJ and Patchett AA (1985) Recent developments in the design of angiotensin-converting enzyme inhibitors. Med Res Rev 5(4):483-531.

[20] Gomez-Monterrey I, Beaumont A, Nemecek P, Roques BP, Fournie-Zaluski MC (1994) New thiol inhibitors of neutral endopeptidase ec 3.4.24.11: Synthesis and enzyme active-site recognition. J Med Chem 37(12):1865-1873.

[21] Supuran C, Scozzafava A, Mastrolorenzo A (2001) Bacterial proteases: Current therapeutic use and future prospects for the development of new antibiotics. Expert Opin. Ther. Patents 11:221–259.

[22] Potempa J and Travis J, *Proteinaes as virulence factors in bacterial diseases and as potential targets for therapeutic intervention with proteinase inhibitors*, in *Proteases as targets for therapy*, K. von der Helm, B.D. Korant, and J.C. Cheronis, Editors. 2000, Springer: Berlin. p. 159-188.

[23] Kim J and Sieburth SM (2004) A silanediol inhibitor of the metalloprotease thermolysin: Synthesi and comparison with a phosphinic acid inhibitor. J Org Chem 69(9):3008-3014.

[24] Gaucher JF, Selkti M, Tiraboschi G, Prange T, Roques BP, Tomas A, Fournie-Zaluski MC (1999) Crystal structures of alpha-mercaptoacyldipeptides in the thermolysin active site: Structural parameters for a zn monodentation or bidentation in metalloendopeptidases. Biochemistry 38(39):12569-12576.

[25] Bartlett PA and Marlowe CK (1987) Possible role for water dissociation in the slow binding of phosphorus-containing transition-state-analogue inhibitors of thermolysin. Biochemistry 26(26):8553-8561.

[26] Morgan B, Scholtz, J. M., Ballinger, M. D., Zipkin, I. D., and Bartlett, P. A. (1991) Differential binding energy: A detailed evaluation of the influence of hydrogen-bonding and hydrophobic groups on the inhibition of thermolysin by phosphorus-containing inhibitors. J. Am. Chem. Soc. 113(1):297 - 307.

[27] Juers DH, Kim J, Matthews BW, Sieburth SM (2005) Structural analysis of silanediols as transition-state-analogue inhibitors of the benchmark metalloprotease thermolysin. Biochemistry 44(50):16524-16528.

[28] Holland DR, Barclay PL, Danilewicz JC, Matthews BW, James K (1994) Inhibition of thermolysin and neutral endopeptidase 24.11 by a novel glutaramide derivative: X-ray structure determination of the thermolysin-inhibitor complex. Biochemistry 33(1):51-56.

[29] Totrov M and Abagyan R (1997) Flexible protein-ligand docking by global energy optimization in internal coordinates. Proteins Suppl 1:215-220.

[30] Halgren TA (1995) Potential energy functions. Curr Opin Struct Biol 5(2):205-210.

[31] Hu X, Balaz S, Shelver WH (2004) A practical approach to docking of zinc metalloproteinase inhibitors. J Mol Graph Model 22(4):293-307.

[32] Wallace AC, Laskowski RA, Thornton JM (1995) Ligplot: A program to generate schematic diagrams of protein-ligand interactions. Protein Eng 8(2):127-134.

[33] Kirchmair J, Ristic S, Eder K, Markt P, Wolber G, Laggner C, Langer T (2007) Fast and efficient in silico 3d screening: Toward maximum computational efficiency of pharmacophore-based and shape-based approaches. J Chem Inf Model 47(6):2182-2196.

[34] Krovat EM, Fruhwirth KH, Langer T (2005) Pharmacophore identification, in silico screening, and virtual library design for inhibitors of the human factor xa. J Chem Inf Model 45(1):146-159.

[35] Schuster D, Laggner C, Steindl TM, Langer T (2006) Development and validation of an in silico p450 profiler based on pharmacophore models. Curr Drug Discov Technol 3(1):1-48.

[36] Steindl TM, Schuster D, Laggner C, Langer T (2006) Parallel screening: A novel concept in pharmacophore modeling and virtual screening. J Chem Inf Model 46(5):2146-2157.

[37] Steindl TM, Schuster D, Wolber G, Laggner C, Langer T (2006) High-throughput structure-based pharmacophore modelling as a basis for successful parallel virtual screening. J Comput Aided Mol Des 20(12):703-715.

[38] Wolber G and Langer T (2005) Ligandscout: 3-d pharmacophores derived from protein-bound ligands and their use as virtual screening filters. J Chem Inf Model 45(1):160-169.

[39] Khan MT, Fuskevag OM, Sylte I (2009) Discovery of potent thermolysin inhibitors using structure based virtual screening and binding assays. J Med Chem 52(1):48-61.

[40] Bursulaya BD, Totrov M, Abagyan R, Brooks CL, 3rd (2003) Comparative study of several algorithms for flexible ligand docking. J Comput Aided Mol Des 17(11):755-763.

[41] Chen H, Lyne PD, Giordanetto F, Lovell T, Li J (2006) On evaluating molecular-docking methods for pose prediction and enrichment factors. J Chem Inf Model 46(1):401-415.

[42] Friesner RA, Banks JL, Murphy RB, Halgren TA, Klicic JJ, Mainz DT, Repasky MP, Knoll EH, Shelley M, Perry JK, Shaw DE, Francis P, Shenkin PS (2004) Glide: A new approach for rapid, accurate docking and scoring. 1. Method and assessment of docking accuracy. J Med Chem 47(7):1739-1749.

[43] Perola E, Walters WP, Charifson PS (2004) A detailed comparison of current docking and scoring methods on systems of pharmaceutical relevance. Proteins 56(2):235-249.

[44] Kroemer RT, Vulpetti A, McDonald JJ, Rohrer DC, Trosset JY, Giordanetto F, Cotesta S, McMartin C, Kihlen M, Stouten PF (2004) Assessment of docking poses: Interactions-based accuracy classification (ibac) versus crystal structure deviations. J Chem Inf Comput Sci 44(3):871-881.

[45] Schapira M, Totrov M, Abagyan R (1999) Prediction of the binding energy for small molecules, peptides and proteins. J Mol Recog 12:177-190.

[46] Hangauer DG, Monzingo AF, Matthews BW (1984) An interactive computer graphics study of thermolysin-catalyzed peptide cleavage and inhibition by n-carboxymethyl dipeptides. Biochemistry 23(24):5730-5741.

[47] Hashida Y and Inouye K (2007) Molecular mechanism of the inhibitory effect of cobalt ion on thermolysin activity and the suppressive effect of calcium ion on the cobalt ion-dependent inactivation of thermolysin. J Biochem 141(6):879-888.

[48] Holden HM and Matthews BW (1988) The binding of l-valyl-l-tryptophan to crystalline thermolysin illustrates the mode of interaction of a product of peptide hydrolysis. J Biol Chem 263(7):3256-3260.

[49] Kitagishi K and Hiromi K (1986) Binding between thermolysin and its specific inhibitor, n-phosphoryl-l-leucyl-l-tryptophan (plt). J Biochem 99(1):191-197.

[50] Kuhn D, Durrschmidt P, Mansfeld J, Ulbrich-Hofmann R (2002) Boilysin and thermolysin in dipeptide synthesis: A comparative study. Biotechnol Appl Biochem 36(Pt 1):71-76.

[51] Monzingo AF and Matthews BW (1984) Binding of n-carboxymethyl dipeptide inhibitors to thermolysin determined by x-ray crystallography: A novel class of transition-state analogues for zinc peptidases. Biochemistry 23(24):5724-5729.

[52] Yasukawa K, Kusano M, Nakamura K, Inouye K (2006) Characterization of gly-d-phe, gly-l-leu, and d-phe as affinity ligands to thermolysin. Protein Expr Purif 46(2):332-336.

[53] Tronrud DE, Monzingo AF, Matthews BW (1986) Crystallographic structural analysis of phosphoramidates as inhibitors and transition-state analogs of thermolysin. Eur J Biochem 157(2):261-268.

[54] Bartlett PA and Marlowe CK (1983) Phosphonamidates as transition-state analogue inhibitors of thermolysin. Biochemistry 22(20):4618-4624.

[55] Bradley Morgan JMS, Marcus D. Ballinger, Ilan D. Zipkin, and Paul A. Bartlett (1991) Differential binding energy: A detailed evaluation of the influence of hydrogen-bonding and hydrophobic groups on the inhibition of thermolysin by phosphorus-containing inhibitors. J. Am. Chem. Soc. 113(1):297-307.

[56] Nishino N and Powers JC (1979) Design of potent reversible inhibitors for thermolysin. Peptides containing zinc coordinating ligands and their use in affinity chromatography. Biochemistry 18(20):4340-4347.

[57] Kam CM, Nishino N, Powers JC (1979) Inhibition of thermolysin and carboxypeptidase a by phosphoramidates. Biochemistry 18(14):3032-3038.

[58] Nishino N and Powers JC (1978) Peptide hydroxamic acids as inhibitors of thermolysin. Biochemistry 17(14):2846-2850.

[59] Cheng F, Zhang R, Luo X, Shen J, Li X, Gu J, Zhu W, Shen J, Sagi I, Ji R, Chen K, Jiang H (2002) Quantum chemistry study on the interaction of the exogenous ligands and the catalytic zinc ion in matrix metalloproteinases. J. Phys. Chem. B 106(17):4552–4559.

Received: January 02, 2011 Revised: August 02, 2011 Accepted: September 02, 2011